Journal of Alloys and Compounds 495 (2010) 121–125

Contents lists available at ScienceDirect

Journal of Alloys and Compounds

journal homepage: www.elsevier.com/locate/jallcom

Synthesis of nanosized (Co, Nb, Sm)-doped SnO_2 powders using co-precipitation method

H. Bastami, E. Taheri-Nassaj*

Department of Materials Science and Engineering, Tarbiat Modares University, P.O. Box 14115-143, Tehran, Iran

ARTICLE INFO

Article history:
Received 20 October 2009
Received in revised form 20 January 2010
Accepted 21 January 2010
Available online 1 February 2010

Keywords:
Samarium oxide
Precipitation
Tin oxide
Nanosized materials
Varistor

ABSTRACT

Synthesis of SnO_2 powder in order to make varistor properties is technologically important. This study aims at examining the process of making nanosized $(98.95-x)SnO_2 + 1CoO + 0.05Nb_2O_5 + xSm_2O_3$ (mol%) ($x = 0.05$, 0.10, 0.20, 0.50, 1.00 and 2.00) powders using co-precipitation method. Some nanopowders were studied through XRD, SEM and FTIR analyses. The XRD patterns displayed only a tetragonal rutile structure for different molar ratios of samarium oxide (Sm_2O_3). The mean crystallite size of the sample doped with 0.05 mol% Sm_2O_3, calcined at 700 °C for 2 h, was about 10 nm. The SEM micrograph of this sample revealed some nanosized spherical particles with a size range of 45–70 nm. The Sm-rich surface prevented the nanoparticles from growing during the calcination at 700 °C.

1. Introduction

Tin oxide is an n-type semiconductor with rutile crystalline structure and so many interesting electronic properties. In the past decades, a great number of papers on new SnO_2-based varistors have been published [1–11]. Non-linear coefficient and breakdown voltage are the most important performance parameters of a varistor. Using nanosized powders in making these varistors causes the breakdown voltage and non-linear coefficient to rise [8,11]. Finding shows that several additives (cations such as Eu [12], Yb [13], Al [14], Co [15], Mn [16], Fe [17], La, Ce, Y [18]) stabilize the SnO_2 surface and lead to a decrease in grain size. Carreño et al. studied the nanosized SnO_2 powders doped with (Ce, La, and Y). Then they have concluded that a supersaturated solid solution yields a nanosized metastable material that will undergo a rare earth cation segregation to the outer surface [18]. This process can effectively be used to control the surface chemistry and subsequently grain growth inhibition.

Nanosized doped SnO_2 powders are obtained by a variety of synthesis techniques such as microwave-assisted solvothermal [12], the polymeric precursor [11], sol–gel hydrothermal [17], hydrothermal [13,18,19], and chemical co-precipitation routes [10,14,16]. Co-precipitation method is a simple way to be followed in preparing homogenous nanosized powders [10,14,16].

The major objective of this study is to prepare nanosized (Co, Nb, Sm)-doped SnO_2 powders by co-precipitation method for varistor applications. The effect of samarium (Sm) concentration on the grain growth of nanosized (Co, Nb)-doped SnO_2 powders will also be discussed.

2. Experimental procedures

2.1. The process of making powder

Analytical grades of $SnCl_4{\cdot}5H_2O$ (Riedel), $Co(NO_3)_2{\cdot}6H_2O$ (BDH), $NbCl_5$ (Merck) and $Sm(NO_3)_3{\cdot}6H_2O$ (Alfa Aesar) were employed. First, two aqueous solutions were prepared according to the molar composition of the investigated systems (Table 1):

Solution one containing: $SnCl_4{\cdot}5H_2O$.
Solution two containing: $Co(NO_3)_2{\cdot}6H_2O$, $Sm(NO_3)_3{\cdot}6H_2O$ and $NbCl_5$.

Nitric acid (HNO_3) was added to the solution two to increase its salt solubility. The solution two was then added to the solution one while stirring. Then NH_4OH was added to the obtained solution to increase the solution pH to 7. To ensure the completion of reactions (hydrolysis and condensation), the system was stirred continuously for 24 h. The precipitates were then filtered and washed using cold deionized water and diethylamine solution to eliminate any chlorine ions [10]. They were then dried at 60 °C for 48 h. The synthesized powders were calcined at 700 °C for 2 h. In order to break the agglomerates, the powders were wet-milled in ethanol media using zirconia balls (2 mm in diameter) for 1 h. The detailed process of powder preparation by chemical route is illustrated in Fig. 1.

2.2. Powder characterization

The crystal structure of the synthesized nanopowders was characterized by X-ray diffraction (XRD) with Cu Kα radiation (Philips X-pert). Also the crystallite size (d) of the products was determined from the X-ray broadening line using Sherrer's

* Corresponding author. Tel.: +98 21 82883306; fax: +98 21 82883381.
E-mail address: taheri@modares.ac.ir (E. Taheri-Nassaj).

0925-8388/$ – see front matter © 2010 Elsevier B.V. All rights reserved.
doi:10.1016/j.jallcom.2010.01.099

Table 1
Molar composition of the investigated systems synthesized by chemical route.

Sample No.	Composition (mol %)			
	SnO_2	CoO	Nb_2O_5	Sm_2O_3
1	100.00	0.00	0.00	0.00
2	99.00	1.00	0.00	0.00
3	98.95	1.00	0.05	0.00
4	98.90	1.00	0.05	0.05
5	98.85	1.00	0.05	0.10
6	98.75	1.00	0.05	0.20
7	98.45	1.00	0.05	0.50
8	97.95	1.00	0.05	1.00
9	96.95	1.00	0.05	2.00

equation [20]:

$$d = \frac{0.9\lambda}{\beta_{sample}\cos(\theta)} \quad (1)$$

where λ is the wavelength (1.54056 Å), θ is the diffraction angle and β_{sample} is the full-width for the half-maximum (FWHM) intensity peak of the powder. The Gaussian–Gaussian relationship was used for instrumental correction [21]:

$$\beta_{sample}{}^2 = \beta_{exp}{}^2 - \beta_{ins}{}^2 \quad (2)$$

where β_{exp} and β_{ins} are the measured FWHMs of the powder and the standard sample, respectively.

Differential thermal analysis (DTA) and thermogravimetric (TG) analysis were performed between room temperature and 1000 °C in air at a heating rate of 5 °C/min using DSC (model L60H1550) and STA (model PL-STA 1500), respectively.

FTIR analyses were carried out in a Thermo Nicolet (model Nexus 670) spectrometer in the wave number range of 400–4000 cm^{-1} for studying the chemical groups on the surface of the samples 1, 2, 3 and 7 dried at 60 °C. The powders morphology was observed by a Philips XL 30 scanning electron microscope.

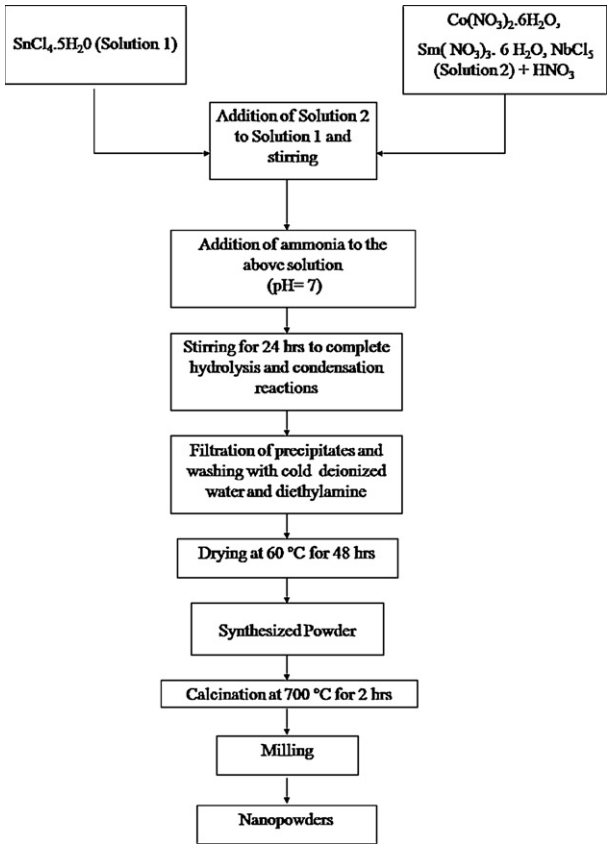

Fig. 1. The typical flow chart of the processing of nanosized SnO_2 powders.

3. Results and discussion

It is well known that tin hydroxide begins to form at pH 0.5 [19]. Furthermore, Sn(IV) tends to hydrolyze in aqueous solution, forming charged and uncharged species of $SnO(OH)_3^-$ at pH ≥ 8 and $SnO(OH)_2$ at pH ≤ 7, respectively [22]. Similar to the study by Seby et al., $SnO(OH)_2$ was first formed in the present study (pH 7) [22]. Then, dopants are formed as their hydroxides on the surface of $SnO(OH)_2$ particles [19]. Cobalt hydroxide, samarium hydroxide and niobium hydroxide were formed at pH ≥ 7 as $Co(OH)_2$, $Sm(OH)_3$ and $Nb(OH)_5$ on the surface of $SnO(OH)_2$ particles during the precipitation. Then they were transformed into their corresponding oxides during the calcination process [19].

$Co(OH)_2$ was formed as follows [23]:

$$Co^{2+} + NH_3 + H_2O + NO_3^- \rightarrow Co(OH)NO_3 \downarrow + NH_4^+ \quad (3)$$

$$Co(OH)NO_3 \downarrow + OH^- \rightarrow Co(OH)_2 \downarrow + NO_3^- \quad (4)$$

$Sm(OH)_3$ was formed at pH ≥ 7 as $Sm(OH)_2(NO_3)$ [24]. Then it was transformed into $Sm(OH)_3$ as follows:

$$Sm(OH)_2(NO_3) \downarrow + OH^- \rightarrow Sm(OH)_3 \downarrow + NO_3^- \quad (5)$$

Also $Nb(OH)_5$ was formed by the following reaction:

$$2NbCl_5 + 10H_2O \rightarrow 2Nb(OH)_5 + 10HCl \quad (6)$$

Therefore, tin hydroxides and other metal hydroxides were formed in the precursor sols during the hydrolysis and condensation reactions [19]. These reactions were completed during the aging for 24 h.

During the calcination, the core $SnO(OH)_2$ was transformed into SnO_2 [19,25] as follows [25]:

$$SnO(OH)_2 \rightarrow SnO_3H_2 \rightarrow Sn_4O_9H_3 \rightarrow SnO_2 \quad (7)$$

Also $SnO(OH)_2$ was dehydrated directly to form SnO_2 as:

$$SnO(OH)_2 \rightarrow SnO_2 + H_2O \quad (8)$$

$Co(OH)_2$, $Sm(OH)_3$ and $Nb(OH)_5$ existing on the surface of SnO_2 were transformed into their corresponding oxides. The formed oxides on the surface of SnO_2 reduce the crystallite size of the nanosized powders. Of course, some cations were expected to be transferred into the interior of SnO_2 and form a solid solution [19,26].

Fig. 2 shows the XRD patterns of the sample doped with 0.05 mol% Sm_2O_3 (No. 4), dried at 60 °C and then calcined at different temperatures (200 °C, 400 °C, 500 °C and 700 °C) for 2 h. The XRD analysis confirmed the presence of tetragonal phase of SnO_2 in the sample dried at 60 °C without heat treatment. Also no other phase besides SnO_2 was observed in the samples calcined at different temperatures. In addition, it was observed that the peak

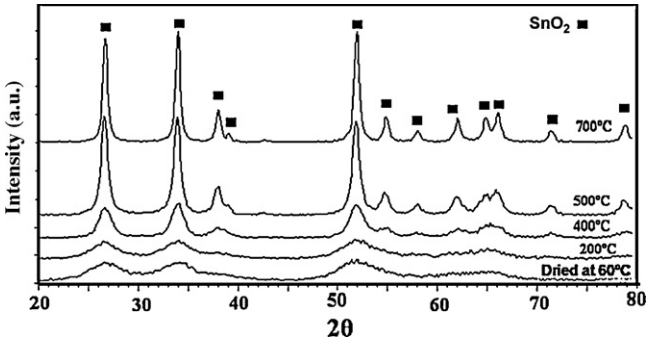

Fig. 2. The XRD patterns of the sample doped with 0.05 mol% Sm_2O_3 dried at 60 °C and then calcined at different temperatures (200 °C, 400 °C, 500 °C and 700 °C) for 2 h.

Table 2
The crystallite size of the sample doped with 0.05 mol% Sm_2O_3 (No. 4) dried at 60 °C and then calcined at different temperatures for 2 h.

Temperature (°C)	60	200	400	500	700
The crystallite size (nm)	2.5	3.3	5.9	6.0	9.9

Table 3
The crystallite size calculated by Scherrer's equation of the undoped and doped SnO_2 with different additives calcined at 700 °C for 2 h.

Sample No.	1	2	3	4	5	6	7	8	9
Crystallite size (nm)	15.6	12.7	12.2	9.9	9.5	8.8	7.5	7.4	7.0

intensity increased with the increasing of calcination temperature. At the same time, broadening of the peak decreased with the increasing of temperature. Several reasons such as burning out of volatiles, increasing of crystallinity and partial sintering between the particles may justify these observations. Particle growth is also affected by calcination temperature.

The crystallite sizes from Scherrer's equation with 2θ near 26.63° are listed in Table 2. The crystallite size of the sample doped with 0.05 mol% Sm_2O_3 (No. 4), dried at 60 °C, was about 2.5 nm. This sample, however, had a large amount of water molecules adsorbed on its surface and also considerable amount of hydroxyl groups in its structure [27]. SnO_2 crystallites grew slowly by the increasing of calcination temperature from 200 °C to 700 °C.

The XRD patterns of different systems (Nos. 1, 2, 3 and 7) calcined at 700 °C for 2 h are illustrated in Fig. 3. The XRD patterns displayed only a tetragonal rutile structure for the undoped SnO_2 (No. 1) and the Co-doped SnO_2 (No. 2). The crystallite size of undoped SnO_2 was 15.6 nm. This value was 12.7 nm for the Co-doped SnO_2. So, it is clear that addition of cobalt oxide reduces the crystallite size of SnO_2, which is in agreement with the findings of other researchers [15,28].

As Table 3 shows, the addition of Nb_2O_5 reduces the crystallite size of Co-doped SnO_2 system. The crystallite size of the sample 3 was 12.2 nm. This is in accordance with the findings of Leite et al. [29,30]. They have reported that the particle growth of SnO_2 can be controlled by addition of Nb_2O_5, which will segregate and contribute to the growth inhibition of SnO_2. This may produce two beneficial effects. The first is on the solute drag, which causes a decrease in particle mobility. The second is a reduction in the driving force. In both cases, the formation of a metastable solid solution

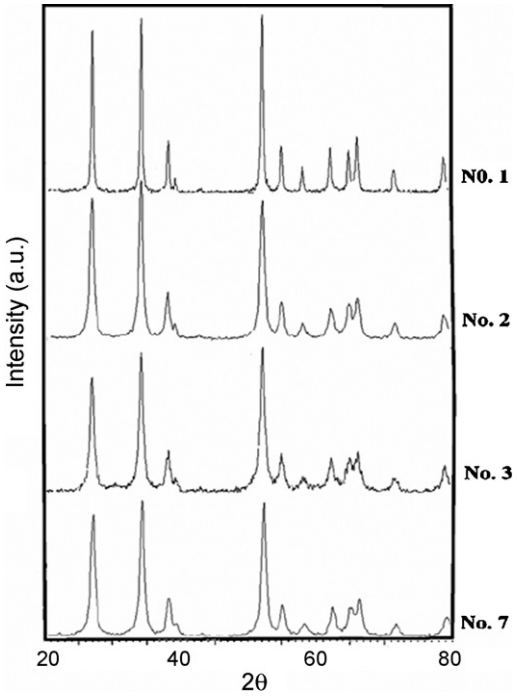

Fig. 3. The XRD patterns of the undoped SnO_2 (No. 1), Co-doped SnO_2 (No. 2), (Co, Nb)-doped SnO_2 (No. 3) and (Co, Nb, Sm)-doped SnO_2 (No. 7) systems calcined at 700 °C for 2 h.

is fundamental to the development of a segregation layer of cations on the particle surface [18,31].

The amount of Sm_2O_3 only affected the crystallite size of nanosized SnO_2 powders and the XRD patterns displayed only a tetragonal rutile structure SnO_2 for the samples 4–9. The addition of Sm_2O_3 reduced the crystallite size of (Co, Nb)-doped SnO_2 and prevented the grains from growing. According to Table 3, small amount of Sm_2O_3 (for example, No. 4) has a great influence in reducing the crystallite size of SnO_2 powders. This effect was observed by Carreño et al. for (Ce, Y, La)-doped SnO_2 prepared by hydrothermal route [18]. They reported that rare earth dopants could inhibit SnO_2 particles from growing at high temperatures.

The solubility limit of three-valence rare earth (RE) ions in SnO_2 is known to be around 0.05 mol% and the excess ions are supposed to segregate at grain boundaries, probably as pyrochlore crystal phase, $RE_2Sn_2O_7$ [32].

Since the ionic radius of Sm^{3+} (0.97 Å) is larger than that of Sn^{4+} (0.71 Å), the substitution of Sn^{4+} by Sm^{3+} leads to distortion of SnO_2 lattice according to the following reaction:

$$Sm_2O_3 \xrightarrow{SnO_2} 2Sm'_{Sn} + 3O_O + V_O^{\bullet\bullet} \quad (9)$$

For this reason, probably the mentioned reaction, which takes place at grain boundaries, will inhibit SnO_2 particles from growing. It is most probable that a metastable solid solution will be formed, yielding a segregation of Sm cations on the surface of SnO_2 [18].

TG/DTA results of the sample doped with 0.05 mol% Sm_2O_3 (No. 4), dried at 60 °C, are shown in Fig. 4. The total weight loss value upon heating to 1000 °C was about 15.5%. An endothermic peak was observed at about 80 °C (with a weight loss of 4%), indicating the physically absorbed water on the surface of the precursor. A great exothermic peak was found at 236 °C on the DTA curve, which may correspond to the decomposition of precursor to form SnO_2 and/or other oxides in the sample. Other peaks appearing between 300 °C and 550 °C correspond to elimination of the nitrates and crystallization of the oxides [10]. No significant weight loss was observed beyond 700 °C. Thus, the synthesized powders were calcined at 700 °C for 2 h.

The detailed FTIR spectra of the samples 1, 2, 3 and 7, dried at 60 °C, are shown in Fig. 5. The strong vibrations extending from

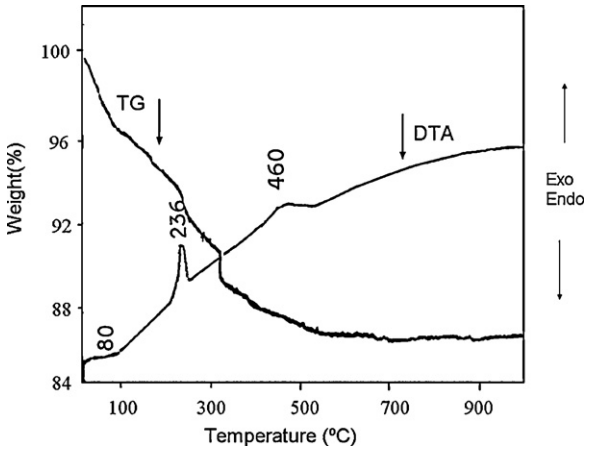

Fig. 4. TG/DTA plots of the sample doped with 0.05 mol% Sm_2O_3 dried at 60 °C in air with the rate of 5 °C/min.

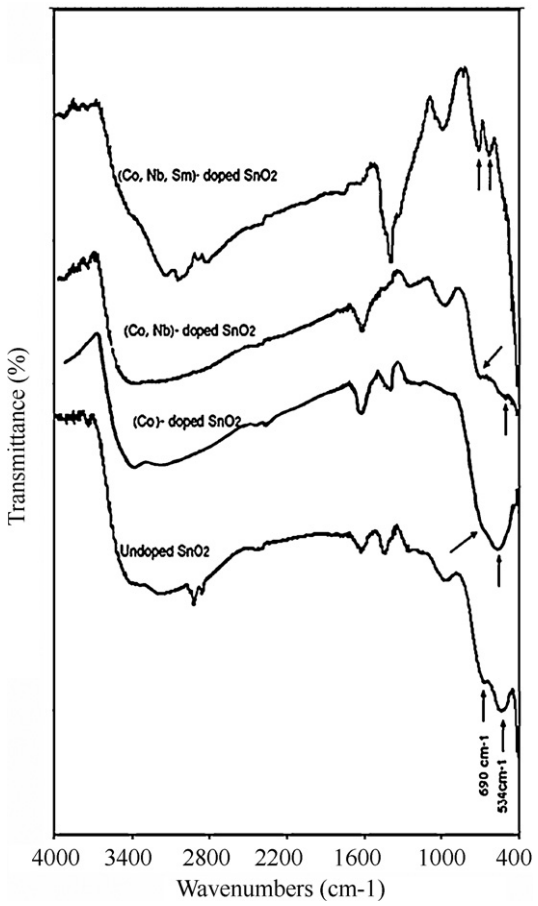

Fig. 5. The IR spectra for undoped SnO_2 (No. 1), Co-doped SnO_2 (No. 2), (Co, Nb)-doped SnO_2 (No. 3) and (Co, Nb, Sm)-doped SnO_2 (No. 7) systems dried at 60 °C.

3500 cm^{-1} to 2500 cm^{-1} indicate the presence of hydrogen bonds involved in O–H oscillators, which may be due to adsorbed water and Sn–OH groups. The peak at 1400 cm^{-1} can be assigned to the bending vibration of NO_3. The peak appeared at 690 cm^{-1} relates to the O–Sn–O bridge functional groups of SnO_2, while the peak appearing at 534 cm^{-1} is due to the terminal oxygen vibration of Sn–OH. These are characteristic vibration absorption peaks of the Sn–O bond in SnO_2 [33]. The peak located at 690 cm^{-1} confirms the presence of SnO_2 as crystalline phase. This is in agreement with the results of the XRD analysis. Addition of dopants changed the positions of two characteristic vibration peaks of the Sn–O bond in SnO_2. The sample doped with cobalt (No. 2) changed the positions of these two peaks to 542 cm^{-1} and 711 cm^{-1}, respectively. The positions of these two peaks were changed to 561 cm^{-1} and 717 cm^{-1}, respectively in the (Co, Nb)-doped SnO_2 (No. 3). There were two peaks located at 652 cm^{-1} and 733 cm^{-1} in the (Co, Nb, Sm)-doped SnO_2 (No. 7). Since FTIR is a technique characterizing the surface of materials [34], the shift of two peaks due to the increasing of dopants may indicate the formation of a metastable solid solution [35], inhibiting the grain growth of nanoparticles.

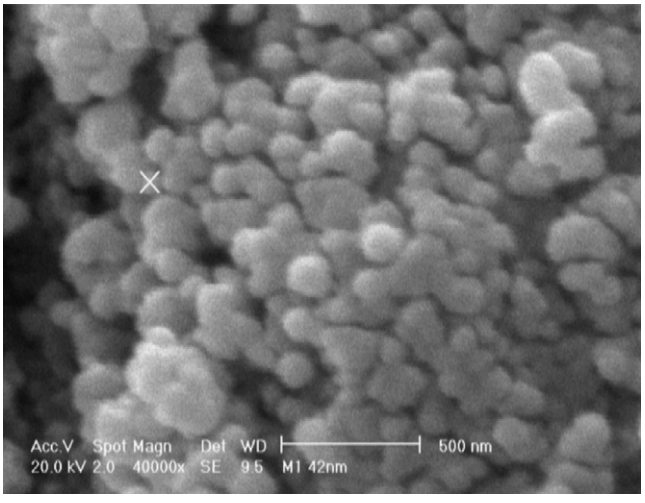

Fig. 6. The SEM micrograph of the sample doped with 0.05 mol% Sm_2O_3 dried at 60 °C and then calcined at 700 °C for 2 h.

The SEM micrograph of the sample doped with 0.05 mol% Sm_2O_3 (No. 4) calcined at 700 °C for 2 h is shown in Fig. 6. As it can be seen, most of the particles are spherical in shape and are in the size range of 45–70 nm.

4. Conclusions

In the present work, nanosized $(98.95-x)SnO_2 + 1CoO + 0.05Nb_2O_5 + xSm_2O_3$ (mol%) (x = 0.05, 0.10, 0.20, 0.50, 1.00 and 2.00) powders were synthesized using chemical route. The obtained results are as follows:

(1) The products had a uniform morphology and narrow particle size distribution.
(2) No other phase besides SnO_2 rutile structure was observed in the samples calcined at different temperatures.
(3) The mean crystallite size of the sample doped with 0.05 mol% Sm_2O_3 calcined at 700 °C for 2 h was about 10 nm.
(4) Addition of Sm_2O_3 reduced the crystallite size of (Co, Nb)-doped SnO_2.
(5) The formation of a metastable solid solution on the surface of nanoparticles reduced the crystallite size of doped samples.
(6) Most of the particles were spherical in shape and were in the size range of 45–70 nm.

References

[1] S.R. Dhage, V. Ravi, O.B. Yang, J. Alloys Compd. 466 (2008) 483–487.
[2] R. Metz, D. Koumeir, J. Morel, J. Pansiot, M. Houabes, M. Hassanzadeh, J. Eur. Ceram. Soc. 28 (2008) 829–835.
[3] R. Parra, J.E. Rodríguez-Páez, J.A. Varela, M.S. Castro, Ceram. Int. 34 (2008) 563–571.
[4] A.B. Glot, A.V. Gaponov, A.P. Sandoval-García, Phys. B: Condens. Matter 405 (2010) 705–711.
[5] P.R. Bueno, J.A. Varela, E. Longo, J. Eur. Ceram. Soc. 28 (2008) 505–529.
[6] J.W. Fan, H.J. Zhao, Y.J. Xi, Y.C. Mu, F. Tang, R. Freer, J. Eur. Ceram. Soc. 30 (2010) 454–548.
[7] J.A. Aguilar-Martínez, M.B. Hernández, M.I. Pech-Canul, A.B. Glot, J. Castillo-Torres, J. Mater. Process. Technol. 209 (2009) 318–323.
[8] M.M. Shahraki, S.A. Shojaee, A. Nemati, M.A. Faghihi-Sani, J. Mater. Sci.-Mater. Electron. 21 (2010) 199–205.
[9] A.V. Gaponov, A.B. Glot, J. Mater. Sci.-Mater. Electron., doi:10.1007/s10854-009r-r9916-1.
[10] A. Mosquera, J.E. Rodringuez-Paez, J.A. Varela, P.R. Bueno, J. Eur. Ceram. Soc. 27 (2007) 3893–3896.
[11] R. Parra, L.A. Ramajo, M.S. Góes, J.A. Varela, M.S. Castro, Mater. Res. Bull. 43 (2008) 3202–3211.
[12] C.-T. Lee, F.-S. Chen, C.-H. Lu, J. Alloys Compd. 490 (2009) 407–411.
[13] D. Jin, X. Yu, H. Yang, H. Zhu, L. Wang, Y. Zheng, J. Alloys Compd. 474 (2009) 557–560.
[14] L. Xi, D. Qian, X. Huang, H.-E. Wang, J. Alloys Compd. 462 (2008) 42–46.
[15] L.M. Fang, X.T. Zu, Z.J. Li, S. Zhu, C.M. Liu, L.M. Wang, F. Gao, J. Mater. Sci.-Mater. Electron. 19 (2008) 868–874.
[16] Z.M. Tian, S.L. Yuan, J.H. He, P. Li, S.Q. Zhang, C.H. Wang, Y.Q. Wang, S.Y. Yin, L. Liu, J. Alloys Compd. 466 (2008) 26–30.
[17] L.M. Fang, X.T. Zu, Z.J. Li, S. Zhu, C.M. Liu, W.L. Zhou, L.M. Wang, J. Alloys Compd. 454 (2008) 261–267.
[18] N.L.V. Carreño, A.P. Maciel, E.R. Leite, P.N. Lisboa-Filho, E. Longo, A. Valentini, L.F.D. Probst, C.O. Paiva-Santos, W.H. Schreiner, Sens. Actuators B 86 (2002) 185–192.
[19] H. Jin, Y. Xu, G. Pang, W. Dong, Q. Wan, Y. Sun, S. Feng, Mater. Chem. Phys. 85 (2004) 58–62.

[20] B.D. Cullity, Elements of X-Ray Diffraction, 2nd edition, Diffraction I: Directions of Diffracted Beams, Addison-Wesley Publishing Company Inc., Massachusetts, 1978, pp. 100–103.
[21] A.P. Hynes, R.H. Doremus, R.W. Siegel, J. Am. Ceram. Soc. 85 (2002) 1979–1987.
[22] F. Seby, M. Potin-Gautier, E. Giffaut, O.F.X. Donard, Geochim. Cosmochim. Acta 65 (2001) 3053.
[23] G. Svehla (Ed.), Vogel's Qualitative Inorganic Analytical, 7th edition, Reactions of the Cations, London, 1996, pp. 126–130.
[24] S.I. Pachenyuk, Russ. Chem. Bull. 48 (1999) 229–238.
[25] H. Yang, W. Jin, L. Wang, Mater. Lett. 57 (2003) 3686–3689.
[26] C. Xu, J. Tamaki, N. Miura, N. Yamazone, J. Mater. Sci. 27 (1992) 963.
[27] A. Toledo- Antonio, R. Gutirrez-Baez, P.J. Sebastian, A. Vazquez, J. Solid State Chem. 174 (2003) 241–248.
[28] G. Korotcenkov, V. Macsanov, V. Brinzari, V. Tolstoy, J. Schwank, A. Cornet, J. Morante, Thin Solid Films 467 (2004) 209–214.
[29] E.R. Leite, I.T. Weber, E. Longo, J.A. Varela, Adv. Mater. 12 (2000) 965–968.
[30] I.T. Weber, R. Andrade, E.R. Leite, E. Longo, Sens. Actuators B 72 (2001) 180.
[31] M.N. Rahman, Ceramic Processing, Sintering and Microstructure Development, Taylor and Francis, Boka Raton/London/New York, 2007, pp. 398–401.
[32] E.A. Morais, S.J.L. Ribeiro, L.V.A. Scalvi, C.V. Santilli, L.O. Ruggiero, S.H. Pulcinelli, Y. Messaddeq, J. Alloys Compd. 344 (2002) 217–220.
[33] J. Zhang, L. Gao, J. Solid State Chem. 177 (2004) 1425–1430.
[34] N. Sergent, P. Gélin, L. Périer-Camby, H. Praliaud, G. Thomas, Sens. Actuators B 84 (2002) 176–188.
[35] G. Brankovic, Z. Brankovik, M.R. Davolos, M. Cilense, J.A. Varela, Mater. Charact. 52 (2004) 243–251.